

**This item is the archived peer-reviewed author-version of:**

Selective laser-assisted synthesis of tubular van der Waals heterostructures of single-layered  $PbI_2$  within carbon nanotubes exhibiting carrier photogeneration

**Reference:**

Sandoval Stefania, Kepic Dejan, Perez del Pino Angel, Gyorgy Eniko, Gomez Andres, Pfannmöller Martin, Van Tendeloo Gustaaf, Ballesteros Belen, Tobias Gerard.-  
Selective laser-assisted synthesis of tubular van der Waals heterostructures of single-layered  $PbI_2$  within carbon nanotubes exhibiting carrier photogeneration  
ACS nano - ISSN 1936-0851 - 12:7(2018), p. 6648-6656

Full text (Publisher's DOI): <https://doi.org/10.1021/ACSNANO.8B01638>

To cite this reference: <https://hdl.handle.net/10067/1531690151162165141>

## Selective Laser-Assisted Synthesis of Tubular van der Waals Heterostructures of Single-Layered Pbl within Carbon Nanotubes Exhibiting Carrier Photogeneration

Stefania Sandoval, Dejan Kepic, Angel Perez del Pino, Eniko Gyorgy, Andres Gomez, Martin Pfanmüller, Gustaaf Van Tendeloo, Belen Ballesteros, and Gerard Tobias

ACS Nano, Just Accepted Manuscript • DOI: 10.1021/acsnano.8b01638 • Publication Date (Web): 05 Jul 2018

Downloaded from <http://pubs.acs.org> on July 5, 2018

### Just Accepted

“Just Accepted” manuscripts have been peer-reviewed and accepted for publication. They are posted online prior to technical editing, formatting for publication and author proofing. The American Chemical Society provides “Just Accepted” as a service to the research community to expedite the dissemination of scientific material as soon as possible after acceptance. “Just Accepted” manuscripts appear in full in PDF format accompanied by an HTML abstract. “Just Accepted” manuscripts have been fully peer reviewed, but should not be considered the official version of record. They are citable by the Digital Object Identifier (DOI®). “Just Accepted” is an optional service offered to authors. Therefore, the “Just Accepted” Web site may not include all articles that will be published in the journal. After a manuscript is technically edited and formatted, it will be removed from the “Just Accepted” Web site and published as an ASAP article. Note that technical editing may introduce minor changes to the manuscript text and/or graphics which could affect content, and all legal disclaimers and ethical guidelines that apply to the journal pertain. ACS cannot be held responsible for errors or consequences arising from the use of information contained in these “Just Accepted” manuscripts.



1  
2  
3  
4  
5  
6  
7 Selective Laser-Assisted Synthesis of Tubular van  
8  
9  
10  
11 der Waals Heterostructures of Single-Layered  $\text{PbI}_2$   
12  
13  
14  
15 within Carbon Nanotubes Exhibiting Carrier  
16  
17  
18  
19 Photogeneration  
20  
21  
22  
23

24 *Stefania Sandoval,<sup>‡</sup> Dejan Kepić,<sup>‡,†</sup> Ángel Pérez del Pino,<sup>\*,‡</sup> Enikő György,<sup>‡</sup> Andrés Gómez,<sup>‡</sup>*  
25  
26 *Martin Pfanmoeller,<sup>§</sup> Gustaaf Van Tendeloo,<sup>§</sup> Belén Ballesteros,<sup>\*,†</sup> and Gerard Tobias<sup>\*,‡</sup>*  
27  
28  
29

30 <sup>‡</sup>Institut de Ciència de Materials de Barcelona (ICMAB-CSIC), Campus UAB, Bellaterra, 08193  
31  
32 Barcelona, Spain  
33  
34

35 <sup>†</sup>Vinča Institute of Nuclear Sciences, P.O. Box 522, University of Belgrade, 11001 Belgrade,  
36  
37 Serbia  
38  
39

40  
41 <sup>§</sup>Electron Microscopy for Materials Research (EMAT), University of Antwerp,  
42  
43 Groenenborgerlaan 171, 2020 Antwerp, Belgium  
44  
45

46  
47 <sup>†</sup>Catalan Institute of Nanoscience and Nanotechnology (ICN2), CSIC and The Barcelona Institute  
48  
49 of Science and Technology, Campus UAB, Bellaterra, 08193 Barcelona, Spain  
50  
51

52 \*Corresponding authors E-mail: gerard.tobias@icmab.es, aperez@icmab.es;  
53  
54 belen.ballesteros@icn2.cat  
55  
56  
57  
58  
59  
60

1  
2  
3 ABSTRACT: The electronic and optical properties of two-dimensional layered materials allow  
4 the miniaturization of nanoelectronic and optoelectronic devices in a competitive manner. Even  
5 larger opportunities arise when two or more layers of different materials are combined. Here we  
6 report on an ultrafast energy efficient strategy, using laser irradiation, which allows bulk  
7 synthesis of crystalline single-layered lead iodide in the cavities of carbon nanotubes by forming  
8 cylindrical van der Waals heterostructures. In contrast to the filling of van der Waals solids into  
9 carbon nanotubes by conventional thermal annealing, which favors the formation of inorganic  
10 nanowires, the present strategy is highly selective towards the growth of monolayers forming  
11 lead iodide nanotubes. The irradiated bulk material bearing the nanotubes reveals a decrease of  
12 the resistivity as well as a significant increase in the current flow upon illumination. Both effects  
13 are attributed to the presence of single-walled lead iodide nanotubes in the cavities of carbon  
14 nanotubes, which dominate the properties of the whole matrix. The present study brings in a  
15 simple, ultrafast and energy efficient strategy for the tailored synthesis of rolled-up single-layers  
16 of lead iodide (*i.e.* single-walled PbI<sub>2</sub> nanotubes), which we believe could be expanded to other  
17 two-dimensional (2D) van der Waals solids. In fact, initial tests with ZnI<sub>2</sub> already reveal the  
18 formation of single-walled ZnI<sub>2</sub> nanotubes, thus proving the versatility of the approach.  
19  
20  
21  
22  
23  
24  
25  
26  
27  
28  
29  
30  
31  
32  
33  
34  
35  
36  
37  
38  
39  
40  
41  
42  
43

44 KEYWORDS: 2D materials, lead iodide, zinc iodide, metal halides, single-walled inorganic  
45 nanotubes, core-shell, encapsulation  
46  
47  
48  
49  
50  
51  
52  
53  
54  
55  
56  
57  
58  
59  
60

1  
2  
3 Two-dimensional layered materials have become a major focus of research because of their  
4 extraordinary properties.<sup>1-4</sup> The high flexibility of single-layered crystals allows rolling them up  
5  
6 to form tubular structures which combine the properties of both two-dimensional and one-  
7  
8 dimensional materials, further expanding their range of application.<sup>5</sup> Strain engineering can be  
9  
10 accomplished by bending two-dimensional materials allowing a fine tuning of their properties.<sup>6</sup>  
11  
12 For example, rolling up MoS<sub>2</sub> sheets induces a tunable semiconducting to metallic phase  
13  
14 transition,<sup>7</sup> and an enhanced photoabsorption when integrated into rolled-up heterostructures  
15  
16 compared to their "flat" configuration.<sup>8</sup> Scrolled graphene/polycarbonate fibers show exotic  
17  
18 telescoping elongation at break 30 times greater than Kevlar.<sup>9</sup> Apart from nanoscrolls, cylindrical  
19  
20 two-dimensional materials (*i.e.* nanotubes) are formed when two parallel edges are seamlessly  
21  
22 joined. Edge states have a strong effect on the electronic properties of two-dimensional  
23  
24 materials.<sup>10</sup> Cylindrical 2D materials are being explored for nanophotonic circuitry because  
25  
26 compressing and channeling of plasmons suffer from scattering at the edges of 2D sheets.<sup>11</sup> From  
27  
28 just these few examples it is clear that single-layered nanotubes, commonly referred to as single-  
29  
30 walled nanotubes, are of great interest for technological applications. However, despite efforts on  
31  
32 the synthesis of nanotubes started more than a decade before the interest on their two-  
33  
34 dimensional "flat" analogues, the amount of single-walled inorganic nanotubes reported to date  
35  
36 is limited because their multi-walled counter parts are favored during synthesis.<sup>12</sup> The synthesis  
37  
38 of elusive single-walled inorganic nanotubes remains as a grand challenge.<sup>13</sup> Therefore,  
39  
40 strategies are needed to fill this gap. A variety of single-walled nanotubes with a high catalytic  
41  
42 performance,<sup>14, 15</sup> not restricted to layered structures in their bulk form, have recently been  
43  
44 synthesized taking advantage of weak interactions between building blocks.<sup>14-16</sup> When it comes  
45  
46 to the synthesis of single-walled nanotubes of van der Waals solids, which are the scope of the  
47  
48  
49  
50  
51  
52  
53  
54  
55  
56  
57  
58  
59  
60

1  
2  
3 present study, we recently reported on the use of carbon nanotubes for the template directed  
4 growth of single-walled materials in their interior.<sup>17</sup> The synthetic strategy proved to be versatile  
5 but requires the use of high temperatures for prolonged periods of time. Furthermore, even under  
6 the best synthetic conditions, a large fraction (at least 35 %) of other nanostructures are formed  
7 in the interior of the carbon nanotubes<sup>18</sup> which could strongly influence the properties. Here we  
8 present an ultrafast, energy efficient and easily scalable approach that allows the selective  
9 synthesis of single-walled lead iodide nanotubes coating the inner walls of carbon nanotubes,  
10 thus forming cylindrical van der Waals heterostructures. By exploiting the properties of van der  
11 Waals heterostructures, a variety of designs and devices emerge.<sup>19, 20</sup> For instance, the  
12 combination of graphene with light-sensitive materials allows the creation of efficient  
13 photodetectors<sup>21</sup> and photoresponsive memory devices.<sup>22</sup> We focused the present study on the  
14 growth of monolayers of lead iodide since this material is of interest not only as a room-  
15 temperature detector of  $\gamma$ - and X-radiation<sup>23</sup> but has also become a strategic material for hybrid  
16 solar cells.<sup>24</sup> Actually, interfacing electrically active graphene with light sensitive lead iodide has  
17 been predicted to substantially enhance its visible light response.<sup>25</sup> To complete the study, the  
18 optoelectronic properties of the resulting heterostructures embedded in the bulk matrix of lead  
19 iodide have been investigated. Remarkably, whereas lead iodide monolayers must be handled  
20 under inert atmosphere to avoid decomposition,<sup>26</sup> the composite materials prepared here can be  
21 handled in air since the carbon shell offers protection to the lead iodide single-layers.  
22  
23  
24  
25  
26  
27  
28  
29  
30  
31  
32  
33  
34  
35  
36  
37  
38  
39  
40  
41  
42  
43  
44  
45  
46  
47  
48

## 49 RESULTS AND DISCUSSION

50  
51 **Laser-Assisted Filling of Carbon Nanotubes.** The encapsulation of materials into the cavities  
52 of previously synthesized carbon nanotubes (CNTs) requires that the filling material either melts  
53  
54  
55  
56  
57  
58  
59  
60

1  
2  
3 or sublimes to allow its incorporation when using high temperature filling strategies.<sup>27-30</sup>  
4  
5 Alternatively, solution filling can be employed but lower filling yields are generally reported and  
6  
7 further processing is required to eliminate the solvent, unless the solvent itself is the chosen  
8  
9 material.<sup>31-34</sup> The controlled synthesis of materials within the cavities of CNTs is getting an  
10  
11 increased attention,<sup>35-37</sup> and for instance MoS<sub>2</sub> and WS<sub>2</sub> nanoribbons have been prepared in this  
12  
13 manner.<sup>27, 38</sup> Laser irradiation of materials can lead to a fast and local increase of the temperature  
14  
15 and arises as a promising alternative to the conventional annealing using furnaces that have been  
16  
17 widely employed to achieve molten phase capillary filling.<sup>39-41</sup> Lead iodide single-walled  
18  
19 nanotubes were grown by laser irradiation of a pellet consisting of open-ended multi-walled  
20  
21 carbon nanotubes (MWCNTs) finely mixed with lead iodide powder. A schematic representation  
22  
23 of the employed process is shown in Figure 1A. Pellets of 1.3 cm in diameter and ca. 0.5 mm in  
24  
25 thickness were prepared by applying a pressure of 10 T to the MWCNT/PbI<sub>2</sub> mixture. A variety  
26  
27 of incident laser fluences (40-100 mJ·cm<sup>-2</sup>) was employed using different number of pulses (10,  
28  
29 100 and 1000 pulses per site). Photothermal simulations were initially performed to obtain  
30  
31 information about the temporal evolution of the temperature reached by the target during the  
32  
33 irradiation with different laser fluences in the 40-100 mJ·cm<sup>-2</sup> range. An idealized system,  
34  
35 composed of a MWCNT immersed in a PbI<sub>2</sub> matrix was employed. Figure 1B shows that the  
36  
37 melting temperature of PbI<sub>2</sub> (T<sub>m</sub> = 410 °C,<sup>42</sup> purple dashed line) would be already exceeded even  
38  
39 at the lowest considered laser fluence (530 °C, 40 mJ·cm<sup>-2</sup>), exhibiting extremely high heating-  
40  
41 cooling rates (up to ca. 2×10<sup>9</sup> °C·s<sup>-1</sup>). In these conditions, the maximum temperature is close to  
42  
43 the temperature previously employed for the synthesis of PbI<sub>2</sub> nanotubes by conventional  
44  
45 annealing treatments (500 °C).<sup>17</sup> The peak temperature is reached at about 4 ns and increases  
46  
47  
48  
49  
50  
51  
52  
53  
54  
55  
56  
57  
58  
59  
60

1  
2  
3 with the applied laser fluence. The maximum achieved temperature with the current strategy  
4  
5 would be ca. 950 °C, after irradiation at 100 mJ·cm<sup>-2</sup>.  
6

7  
8 **Structural Analysis of Cylindrical van der Waals Heterostructures.** Analyses of the laser  
9  
10 irradiated samples by back-scattered scanning electron microscopy (SEM), which provides Z-  
11  
12 contrast images of the samples, indicated that filling of the CNTs occurred in the whole range of  
13  
14 laser fluences and number of accumulated pulses (Figure S1). A small fraction of the pellet  
15  
16 irradiated at different laser fluences and pulses was gently scratched and characterized by high-  
17  
18 angle annular dark field (HAADF) imaging in high resolution scanning transmission electron  
19  
20 microscopy (STEM). Regardless of the laser fluence (40-100 mJ·cm<sup>-2</sup>) and pulses employed (10,  
21  
22 100 and 1000 pulses) the vast majority of MWCNTs that were filled with PbI<sub>2</sub> presented the  
23  
24 characteristic contrast of PbI<sub>2</sub> nanotubes and a minority of them revealed the presence of PbI<sub>2</sub>  
25  
26 nanowires. A representative HAADF-STEM image providing a general view of the sample  
27  
28 prepared at 80 mJ·cm<sup>-2</sup> fluence and 1000 pulses is presented in Figure 2A and additional images  
29  
30 are included in Figure S2. Since HAADF-STEM imaging is strongly dependent on the atomic  
31  
32 number Z,<sup>43</sup> heavy elements such as Pb (Z = 82) and I (Z = 53) appear with a bright contrast,  
33  
34 whereas carbon (Z = 6) appears as pale grey. As it can be seen in the images, the inner cavities of  
35  
36 the hosting CNTs are contoured by bright lines indicating the successful formation of single-  
37  
38 walled PbI<sub>2</sub> nanotubes in their interior. At low laser fluences the observed inorganic PbI<sub>2</sub>  
39  
40 presented a more defective/fractioned structure than at higher fluences. Figure S3 shows  
41  
42 HAADF-STEM images of the sample prepared at 40 mJ·cm<sup>-2</sup> fluence and 1000 pulses. Visual  
43  
44 inspection of the irradiated pellet already reflects the cumulative effect of increasing the number  
45  
46 of laser pulses (Figure S4). Thus, the highest amount of PbI<sub>2</sub> filled MWCNTs would be expected  
47  
48 at 1000 pulses. A quantitative determination of the ratio between filled and empty MWCNTs is  
49  
50  
51  
52  
53  
54  
55  
56  
57  
58  
59  
60



1  
2  
3 not possible since the irradiated areas were manually scratched for HAADF-STEM inspection.  
4  
5 During this process non-irradiated areas could be also collected and imaged.  
6

7  
8 It is worth stressing that all the inorganic  $\text{PbI}_2$  nanotubes imaged in the present study (over  
9  
10 1000) are single-walled. The presence of multi-walled  $\text{PbI}_2$  was not observed regardless of the  
11  
12 laser fluence and pulses employed. Two additional samples were prepared to assess whether the  
13  
14 use of higher fluence ( $200 \text{ mJ}\cdot\text{cm}^{-2}$ , 1000 pulses) or number of pulses (10000 pulses,  $100 \text{ mJ}\cdot\text{cm}^{-2}$ )  
15  
16 would favor the formation of multi-walled  $\text{PbI}_2$ . Despite the extremely high temperature  
17  
18 developed in the material at  $200 \text{ mJ}\cdot\text{cm}^{-2}$  (ca.  $1700 \text{ }^\circ\text{C}$  according to simulation, Figure S5) and  
19  
20 much longer irradiation time, analyses of the irradiated areas by HAADF-STEM revealed the  
21  
22 absence of multi-walled nanotubes.  
23  
24  
25

26 We also investigated the stability of the confined monolayers one year after their synthesis.  
27  
28 Samples were kept under ambient conditions, thus exposed to humidity and air. Despite  $\text{PbI}_2$  is a  
29  
30 rather unstable material which can decompose gradually in wet air,<sup>26</sup> HAADF-STEM imaging  
31  
32 reveals the presence of  $\text{PbI}_2$  nanotubes still inside the cavities of CNTs with only partial damage  
33  
34 in some areas (Figure S6;  $80 \text{ mJ}\cdot\text{cm}^{-2}$  fluence and 1000 pulses). This microscopy analysis  
35  
36 confirms that MWCNTs not only act as templates for the growth of tubular inorganic  
37  
38 nanostructures, but also offer shielding and protection of the inner  $\text{PbI}_2$  nanotubes from the  
39  
40 external environment. This is a major advantage compared to physical vapor deposition grown  
41  
42  $\text{PbI}_2$  layers where the synthetic process, conservation, and testing has to be carried out under an  
43  
44 inert atmosphere ( $\text{N}_2$ ) or under vacuum conditions.<sup>26</sup> Further analysis with a state-of-the-art  
45  
46 aberration corrected electron microscope was performed on the one year old sample to confirm  
47  
48 the presence of  $\text{PbI}_2$  monolayers. Figure 2B shows a high resolution HAADF-STEM image of an  
49  
50 individual  $\text{PbI}_2$  nanotube confined within a MWCNT. Due to the tubular nature of the material,  
51  
52  
53  
54  
55  
56  
57  
58  
59  
60

1  
2  
3 brighter lines are observed at the edges indicating a higher density of atoms in the projected  
4 image, while the central area presents a lower contrast due to the presence of a hollow cavity.  
5  
6 The  $\text{PbI}_2$  nanotube wall thickness (ca. 0.4 nm), indicated in the figure by orange lines, is in  
7 agreement with that of an individual layer of  $\text{PbI}_2$ .<sup>44</sup> Both the curvature and the crystallinity of  
8 the structure are well appreciated.  
9  
10  
11  
12  
13

14 In order to provide direct evidence of the superiority of the laser-assisted approach compared  
15 to the conventional thermal annealing treatment for the growth of single-walled materials in the  
16 interior of CNTs, additional samples were prepared. MWCNT/ $\text{PbI}_2$  mixtures were furnace  
17 annealed maintaining the synthesis conditions previously reported for the growth of single-  
18 walled  $\text{PbI}_2$  within CNTs,<sup>17</sup> and the resulting sample was also analyzed by HAADF-STEM  
19 (Figure S7). Visual inspection of the images shows clear differences between the structures  
20 grown within MWCNTs by laser irradiation (Figure 2, Figure S2) and conventional thermal  
21 annealing (Figure S7). In the case of conventional thermal treatments there is a strong tendency  
22 towards the formation of nanowires of  $\text{PbI}_2$  (orange arrows), observed as continuous bright bars  
23 inside the MWCNTs. On the contrary, the presence of long  $\text{PbI}_2$  inorganic nanotubes (green  
24 arrows) covering the entire interior of CNTs was predominant when laser treatments were  
25 carried out. It is worth noting that when conventional annealing treatments are performed, metal  
26 halide nanotubes and nanorods tend to coexist in an individual CNT forming nanotube-nanorod  
27 junctions<sup>17</sup> and therefore, metal halide nanotubes above 35 nm in length are already considered  
28 as “long” specimens.<sup>18</sup> Remarkably, the majority of single-walled  $\text{PbI}_2$  nanotubes prepared by  
29 laser irradiation have lengths of hundreds of nanometers.  
30  
31  
32  
33  
34  
35  
36  
37  
38  
39  
40  
41  
42  
43  
44  
45  
46  
47  
48  
49  
50

51 HAADF-STEM analyses were performed to quantitatively determine the production yield of  
52 single-walled  $\text{PbI}_2$  nanotubes. The yield turned out to be more than four times higher when using  
53  
54  
55  
56  
57  
58  
59  
60

1  
2  
3 laser irradiation (ca. 94 % of filled CNTs contained PbI<sub>2</sub> nanotubes; 80 mJ·cm<sup>-2</sup> fluence and  
4  
5 1000 pulses) compared to conventional thermal annealing (21.7 % of filled CNTs contained PbI<sub>2</sub>  
6  
7 nanotubes). Similar production yields, within experimental error, were observed when  
8  
9 employing 100 mJ·cm<sup>-2</sup> fluence (1000 pulses). From these analyses it is clear that laser treatment  
10  
11 leads to the selective formation of high quality single-walled PbI<sub>2</sub> nanotubes, their dimensions  
12  
13 depending on the length and inner diameter of the hosting carbon nanotubes.  
14  
15

16  
17 It should be remarked that hitherto such selective growth of inner metal halide nanotubes has  
18  
19 not been obtained through conventional annealing treatments. Actually, using the same annealing  
20  
21 temperature (500 °C ± 25 °C) a similar yield has been reported for the production of single-  
22  
23 walled ZnI<sub>2</sub> inside CNTs<sup>18</sup> (21.4 %; mp(ZnI<sub>2</sub>) = 446 °C,<sup>42</sup> T<sub>filling</sub> = 475 °C), and even for the  
24  
25 formation of multi-walled PbI<sub>2</sub> and BiI<sub>3</sub> in the cavities of WS<sub>2</sub> nanotubes<sup>45</sup> (around 20 % of  
26  
27 iodide nanotubes; mp(PbI<sub>2</sub>) = 410 °C,<sup>42</sup> mp(BiI<sub>3</sub>) = 408.6 °C,<sup>42</sup> T<sub>filling</sub> = 500 °C). Prolonged 14-30  
28  
29 days of annealing were employed when using WS<sub>2</sub> nanotubes as templates.<sup>45, 46</sup> A higher amount  
30  
31 of single-walled nanotubes within CNTs has been recently reported upon increasing the  
32  
33 temperature of annealing, from 21.4 % at 475 °C to 64.9 % at 1000 °C, for the van der Waals  
34  
35 solid ZnI<sub>2</sub>.<sup>18</sup> Nevertheless, not only the production yield is still lower than the one reported here  
36  
37 (for PbI<sub>2</sub> using laser) but also much longer tubular structures are obtained by laser irradiation.  
38  
39  
40  
41

42  
43 Considering that the temperature employed for the synthesis of PbI<sub>2</sub> nanotubes by conventional  
44  
45 annealing (500 °C) is considerably lower than the temperature reached by laser irradiation at 80  
46  
47 mJ·cm<sup>-2</sup> and 100 mJ·cm<sup>-2</sup> (796 °C and 953 °C respectively, as per photothermal simulations  
48  
49 reported in Figure 1), additional thermal treatments of MWCNT/PbI<sub>2</sub> pellets were carried out at  
50  
51 these temperatures. Under these conditions the presence of inorganic nanostructures within  
52  
53  
54  
55  
56  
57  
58  
59  
60

1  
2  
3 MWCNTs was barely observed (Figure S8). Furthermore, the few observed structures did not  
4  
5 show selectivity towards the formation of inorganic nanotubes.  
6

7  
8 Raman spectroscopy analyses were performed to determine the quality of MWCNTs' structure  
9  
10 after laser irradiation. Laser irradiation induces high temperature thermal cycles, which can lead  
11  
12 to the formation of structural defects, premelting and even amorphisation of MWCNTs.<sup>47</sup> Raman  
13  
14 spectra recorded on both non-irradiated and irradiated MWCNT/PbI<sub>2</sub> areas were fitted using four  
15  
16 Lorentzian and one Gaussian function in the range from 1100-1700 cm<sup>-1</sup> (Figure 3, Figure S9).  
17  
18 The I<sub>D</sub>'/I<sub>G</sub> ratio was calculated to account for structural variations (Table S1). Despite a slight  
19  
20 increase in the I<sub>D</sub>'/I<sub>G</sub> ratio in samples treated with fluences of 80 and 100 mJ·cm<sup>-2</sup>, this variation  
21  
22 does not represent a significant change in the morphology and amount of structural defects of the  
23  
24 MWCNTs. Therefore, the encapsulation of PbI<sub>2</sub> within the hollow core of MWCNTs is expected  
25  
26 to take place through the open-ends rather than through structural defects on the MWCNT walls.  
27  
28  
29

30  
31 **Mechanism of Formation of Tubular van der Waals Heterostructures.** As mentioned  
32  
33 above, the laser assisted synthesis is highly selective towards the formation of PbI<sub>2</sub> nanotubes  
34  
35 with respect to PbI<sub>2</sub> nanowires. Furthermore, when PbI<sub>2</sub> nanotubes are present within the cavities  
36  
37 of MWCNTs a 100% selectivity towards the formation of single-walled PbI<sub>2</sub> was observed;  
38  
39 multi-walled PbI<sub>2</sub> were not detected. The reason behind the high selectivity towards the  
40  
41 formation of monolayered PbI<sub>2</sub> nanotubes with respect to their multi-walled counterparts lies in  
42  
43 the physico-chemical properties of the template employed (Elicarb<sup>®</sup> MWCNTs) rather than from  
44  
45 the method employed for their synthesis. In the first report on the growth of PbI<sub>2</sub> nanotubes using  
46  
47 the conventional thermal annealing method, the formation of multi-walled PbI<sub>2</sub> was also not  
48  
49 observed.<sup>17</sup> In a more recent study, from over 600 inorganic metal halide nanotubes grown  
50  
51 within MWCNTs (CeI<sub>3</sub>, CeCl<sub>3</sub>, TbCl<sub>3</sub> and ZnI<sub>2</sub>) only in one case an inorganic nanotube bearing  
52  
53  
54  
55  
56  
57  
58  
59  
60

1  
2  
3 more than one layer was reported (a triple-walled nanotube of ZnI<sub>2</sub>), the rest being single-walled  
4  
5 (*i.e.* over 99.8 % selectivity).<sup>18</sup> The employed MWCNTs in all these studies have internal  
6  
7 diameters up to 9 nm, with a larger proportion of nanotubes between 4 and 6 nm.<sup>18</sup> A PbI<sub>2</sub>  
8  
9 monolayer has a larger thickness than atomically thin van der Waals solids such as graphene. As  
10  
11 a consequence the formation of multi-walled metal halides within the relatively small cavities of  
12  
13 the MWCNTs employed in this study might not be favored because it would have high strain  
14  
15 energy. In contrast, the formation of multi-walled metal halide nanotubes has been observed in  
16  
17 the cavities of WS<sub>2</sub> nanotubes, which have larger diameters.<sup>45, 46</sup> The diameter of the host is not  
18  
19 the only parameter that needs to be taken into account when forming tubular core-shell  
20  
21 heterostructures. For instance, using a semi-empirical model, it was shown that PbI<sub>2</sub> nanotubes  
22  
23 became stable within the core of MoS<sub>2</sub> nanotubes only above a critical core diameter of the host  
24  
25 (>12 nm); below this diameter the PbI<sub>2</sub> was found to crystallize as nanowires.<sup>45</sup> These model  
26  
27 calculations were in agreement with the experimental observations.<sup>45</sup> In contrast, when using  
28  
29 CNTs as templates the formation of PbI<sub>2</sub> nanotubes occurs well below 12 nm.  
30  
31  
32  
33  
34

35 Molten phase capillary wetting has been suggested as the growth mechanism of a large variety  
36  
37 of metal halide nanowires inside the cavities of carbon nanotubes, using the methodology that we  
38  
39 are referring to as “conventional thermal annealing treatment”. Following this approach, PbI<sub>2</sub>  
40  
41 nanowires were grown by Flahaut *et al.* inside the cavities of single-walled and double-walled  
42  
43 carbon nanotubes back in 2006.<sup>48</sup> Theoretical calculations on the capillary imbibition of PbI<sub>2</sub>  
44  
45 melt into inorganic and carbon nanotubes suggest that when the ionic melt wets the interior of  
46  
47 the host nanotube forming a convex meniscus a PbI<sub>2</sub> nanowire will be obtained on cooling,  
48  
49 whereas when a concave meniscus is created by capillary wetting an inorganic PbI<sub>2</sub> nanotube  
50  
51 will be formed on cooling.<sup>49</sup>  
52  
53  
54  
55  
56  
57  
58  
59  
60

1  
2  
3 Other mechanisms have been employed for the growth of layered metal halides. Large-scale  
4 2D PbI<sub>2</sub> monolayers and few-layers have been recently grown on a SiO<sub>2</sub>/Si substrate by a  
5 catalyst-free physical vapor deposition process.<sup>26</sup> In this case, PbI<sub>2</sub> was added to a ceramic boat  
6 and the substrate was placed on top. The furnace was then annealed to 683 K (409.85 °C) at a  
7 rate of 24 K/min for short periods of time (1-3 min). Vapor deposition of PbI<sub>2</sub> onto the substrate  
8 was observed under these conditions.<sup>26</sup> In another study, Tenne *et al.* used electron beam  
9 irradiation of a powder of SbI<sub>3</sub> to create tubular core-shell structures using WS<sub>2</sub> as templates.  
10 Evaporation followed by recrystallization was suggested as the growth mechanism.<sup>45</sup>  
11  
12  
13  
14  
15  
16  
17  
18  
19  
20  
21

22 Despite further studies are needed, we reason that the laser irradiation method might favor the  
23 vapor deposition of PbI<sub>2</sub> and enhance the formation of PbI<sub>2</sub> nanotubes, whereas capillary wetting  
24 would be predominant by the conventional thermal annealing, the latter favoring the formation of  
25 nanowires. In fact, molecular dynamic simulations reveal that insertion of molten PbI<sub>2</sub> into CNTs  
26 would lead to the formation of PbI<sub>2</sub> nanowires because a convex meniscus is obtained due to the  
27 weak wetting of the CNTs by the ionic melt.<sup>49</sup> Therefore an alternative growth mechanism  
28 should be proposed to justify the high yield of single-walled PbI<sub>2</sub> obtained by the laser process.  
29 Taking into account that vapor deposition has been employed for the growth of monolayer PbI<sub>2</sub>  
30 onto a SiO<sub>2</sub>/Si substrate at ca. 410 °C,<sup>26</sup> it seems plausible that the same growth mechanism takes  
31 place during laser processing. Besides, after irradiation of the MWCNT/PbI<sub>2</sub> pellet deposition of  
32 PbI<sub>2</sub> is observed on the quartz window of the vacuum chamber, indicating the presence of PbI<sub>2</sub>  
33 vapor during the process. Nevertheless, molten phase capillary wetting cannot be ruled out since  
34 resolidified PbI<sub>2</sub> is also observed in the irradiated areas. After the filling experiment using the  
35 conventional thermal annealing, the carbon nanotubes are embedded within resolidified PbI<sub>2</sub>,  
36 indicating that the carbon nanotubes were in direct contact with the PbI<sub>2</sub> melt during the  
37  
38  
39  
40  
41  
42  
43  
44  
45  
46  
47  
48  
49  
50  
51  
52  
53  
54  
55  
56  
57  
58  
59  
60

1  
2  
3 annealing step. Therefore, molten phase capillary wetting seems to be favored when using this  
4 approach. As mentioned, in the conventional annealing treatment a mixture of CNTs and  $\text{PbI}_2$  is  
5 placed on one end of a silica ampoule and vacuum-sealed. After the heating step, a slight  
6 deposition of  $\text{PbI}_2$  is actually observed at the opposite end (cool end during the annealing), far  
7 away from the CNTs. Therefore under these experimental conditions vapor deposition would be  
8 less favored.  
9

10  
11  
12 **Optoelectronic Properties.** Next, the electronic properties of the prepared materials were  
13 investigated. Local resistance characterization of  $\text{PbI}_2$  and MWCNT/ $\text{PbI}_2$  pellets irradiated with a  
14 laser fluence of  $80 \text{ mJ}\cdot\text{cm}^{-2}$  and 1000 accumulated pulses were performed by conducting AFM  
15 (Figure 4). Resistance map histograms, presented in Figure 4A, clearly show that a non-  
16 irradiated MWCNT/ $\text{PbI}_2$  pellet is less resistive than a pellet of  $\text{PbI}_2$  (six orders of magnitude  
17 difference in resistance), due to the conducting nature of the MWCNTs. Both, resistance map  
18 images (a1 and a2) and corresponding histograms indicate a pronounced decrease on the  
19 resistance of the MWCNT/ $\text{PbI}_2$  pellet (blue histogram; average resistance of 3 k $\Omega$ ) after laser  
20 irradiation (red histogram; avg. resistance 1 k $\Omega$ ). The non-irradiated material consists of a  
21 mixture of bulk  $\text{PbI}_2$  and empty MWCNTs. The irradiated sample still contains a  $\text{PbI}_2$  matrix but  
22 the MWCNTs become filled with concentric single-layers of  $\text{PbI}_2$ . Therefore, the higher  
23 conductivity observed after irradiation could arise from the formed heterostructures of  
24  $\text{PbI}_2$ @MWCNTs. This hypothesis was confirmed by analyzing an additional control sample,  
25 prepared by irradiating a pellet of bulk  $\text{PbI}_2$  under the same laser conditions ( $80 \text{ mJ}\cdot\text{cm}^{-2}$  and  
26 1000 pulses). Conducting AFM measurements on the irradiated  $\text{PbI}_2$  did not present such an  
27 increase in conductivity but rather revealed some fading of its resistance. This was probably  
28  
29  
30  
31  
32  
33  
34  
35  
36  
37  
38  
39  
40  
41  
42  
43  
44  
45  
46  
47  
48  
49  
50  
51  
52  
53  
54  
55  
56  
57  
58  
59  
60

1  
2  
3 caused by the formation of larger crystals, with an obvious decrease of grain boundaries, after  
4 laser-induced melting and resolidification processes.  
5  
6

7  
8 Lead iodide being a light sensitive material and taking into account the interest that van der  
9  
10 Waals heterostructures of conductive (CNTs) and optically active ( $\text{PbI}_2$ ) materials have for the  
11 miniaturization of devices,<sup>20</sup> we characterized the optoelectronic response of the material.  
12  
13 Electrical characterization of laser irradiated MWCNT/ $\text{PbI}_2$  was carried out through current-  
14  
15 voltage spectroscopy loops in dark conditions and under illumination with a blue light emitting  
16  
17 diode (LED, ca. 465 nm dominant wavelength). As it can be observed in Figure 4B, the current  
18  
19 flowing through the material considerably increases upon illumination, accounting for significant  
20  
21 carrier photogeneration processes. Remarkably this effect was not observed in a pellet of bulk  
22  
23  $\text{PbI}_2$  where no difference in the conductivity was registered upon illumination. A schematic  
24  
25 representation of the experimental set-up employed for the conducting AFM measurements is  
26  
27 presented in Figure 4C. It is worth noting that despite single-walled lead iodide nanotubes are  
28  
29 protected by the concentric graphene layers of carbon nanotubes, they remain optically active.  
30  
31 Actually, according to Geim *et al.* each graphene layer is expected to add 2.3 % opacity,<sup>50</sup>  
32  
33 therefore since the employed CNTs have an average of nine concentric graphene walls (Figure  
34  
35 S10), about 79.3 % of incident light is expected to reach the inner cavities of the carbon  
36  
37 nanotubes, where lead iodide is present. Based on DFT calculations a substantial enhancement of  
38  
39 the visible light response would be expected when interfacing electrically active graphene with  
40  
41 single-layers of  $\text{PbI}_2$  nanosheets.<sup>25</sup>  
42  
43  
44  
45  
46  
47  
48

49 **Versatility of the Laser-Assisted Filling of Carbon Nanotubes.** To complete the study we  
50 investigated whether it was possible to expand the laser-assisted synthesis of tubular van der  
51  
52 Waals heterostructures to other materials. For this purpose, the same strategy that was employed  
53  
54  
55  
56  
57  
58  
59  
60



1  
2  
3 for the formation of  $\text{PbI}_2$ @MWCNTs was tested using  $\text{ZnI}_2$  as filling material and MWCNTs as  
4 hosts. Open-ended MWCNTs were finely ground with zinc iodide powder, and a pellet of 1.3 cm  
5 in diameter and ca. 0.5 mm in thickness was prepared by applying a pressure of 10 T to the  
6 MWCNT/ $\text{ZnI}_2$  mixture. The pellet was irradiated with an incident laser fluence of  $100 \text{ mJ}\cdot\text{cm}^{-2}$   
7 using 1000 pulses. The laser-irradiated area was gently scratched and the collected sample was  
8 deposited onto a lacey carbon support grid for TEM inspection. As it can be seen in Figure 5,  
9 HAADF-STEM imaging confirmed the successful formation of single-walled  $\text{ZnI}_2$  nanotubes  
10 inside the cavities of MWCNT (see Figure S11 for additional images). The intensity profile  
11 acquired along the red arrow (right panel in Figure 5) is in agreement with the presence of a  
12 single-walled nanotube. The growth of inorganic nanotubes of  $\text{ZnI}_2$  within the cavities of  
13 MWCNTs provides evidence of the versatility of the laser-assisted methodology presented  
14 herein for the synthesis of tubular van der Waals heterostructures.  
15  
16  
17  
18  
19  
20  
21  
22  
23  
24  
25  
26  
27  
28  
29  
30  
31  
32

### 33 CONCLUSIONS

34  
35 We explored an ultrafast energy efficient methodology for the synthesis of tubular van der  
36 Waals heterostructures composed of single-walled lead iodide nanotubes along the inner walls of  
37 multi-walled carbon nanotubes. The synthetic strategy, which benefits from fast thermal cycles  
38 induced by pulsed laser irradiation, is highly selective towards the growth of single-walled lead  
39 iodide nanotubes. This contrasts to previous reports on the encapsulation of van der Waals metal  
40 halides into the cavities of CNTs where the formation of nanowires is favored by conventional  
41 thermal annealing. It is worth pointing out that whereas core-shell nanostructures of carbon and  
42 inorganic materials have been traditionally prepared by filling carbon nanotubes, more recently a  
43 complementary synthetic strategy has received widespread attention where previously  
44  
45  
46  
47  
48  
49  
50  
51  
52  
53  
54  
55  
56  
57  
58  
59  
60

1  
2  
3 synthesized nanowires are covered by a graphene sheet.<sup>51</sup> The laser methodology employed here  
4  
5 results in the formation of cylindrical van der Waals heterostructures of a conductive (CNT) and  
6  
7 a light sensitive material (PbI<sub>2</sub>), which conductivity can be tuned upon illumination, caused by  
8  
9 the photogeneration of carriers. The carbon shell offers protection and stability to the monolayers  
10  
11 of air sensitive lead iodide<sup>26</sup> thus allowing its manipulation under ambient conditions.  
12  
13 Furthermore, since the single-layers of lead iodide easily accommodate to the inner diameter and  
14  
15 shape of the CNTs, it should allow strain engineering of van der Waals solids. It is well  
16  
17 established that the properties of single-layered crystals can be tuned by inducing strain, for  
18  
19 instance upon bending.<sup>6</sup> Versatility of the laser-assisted synthesis was confirmed by growing  
20  
21 single-walled ZnI<sub>2</sub> within MWCNTs. We believe that the use of laser irradiation, which is widely  
22  
23 employed in industrial processes, will allow the encapsulation of a large variety of materials into  
24  
25 CNTs including for the formation of van der Waals heterostructures in a simple, fast, and energy  
26  
27 efficient manner.  
28  
29  
30  
31  
32  
33  
34

## 35 METHODS

36  
37 **MWCNTs Purification.** MWCNTs (CVD, Thomas Swan & Co. Ltd.) were firstly steam  
38  
39 purified to remove amorphous carbon and catalyst nanoparticles, as previously reported.<sup>52</sup> This  
40  
41 procedure involves placing MWCNTs in a furnace at 900 °C for 5 h with a constant flow of  
42  
43 steam/argon mixture. Being a mild oxidizer, steam oxidizes graphitic shell around catalyst  
44  
45 nanoparticles and opens the nanotubes' ends. Subsequently, the sample was placed into a round-  
46  
47 bottom flask and refluxed with 6 M HCl at 110 °C for 6 h to remove the catalyst particles, cooled  
48  
49 down and filtered through 0.2 μm polycarbonate membrane filters, washing with distilled water  
50  
51 until neutral pH was reached and dried.  
52  
53  
54  
55  
56  
57  
58  
59  
60

1  
2  
3       **Laser-assisted Synthesis of PbI<sub>2</sub> Nanotubes.** 36 mg of purified MWCNTs were mixed with  
4  
5 210 mg of PbI<sub>2</sub> (Strem Chemicals Inc.) and well homogenized using an agate pestle and mortar  
6  
7 inside an argon-filled glovebox. Pellets with 1.3 cm in diameter and ca. 0.5 mm in thickness  
8  
9 were formed applying a pressure of 10 T to the MWCNT/PbI<sub>2</sub> mixture. An additional pellet  
10  
11 containing 260 mg of PbI<sub>2</sub> was prepared to be employed as a reference.  
12  
13

14  
15       Pulsed laser treatments of MWCNT/PbI<sub>2</sub> pellets were carried out by means of a Nd:YAG laser  
16  
17 system (266 nm, 3 ns pulse duration, 10 Hz pulse repetition rate; Brilliant model from Quantel).  
18  
19 The experiments were performed inside a vacuum chamber at a pressure of 10<sup>-4</sup> Pa to avoid  
20  
21 oxidation reactions. A quartz window was placed on top of the pellet to prevent direct deposition  
22  
23 of PbI<sub>2</sub> onto the optical window of the vacuum chamber. The irradiations were done by focusing  
24  
25 the laser beam onto the sample surface, creating 1×1 mm<sup>2</sup> homogeneous squared spots. The  
26  
27 distance between two adjacent irradiated spots was set to be 1 mm. Different samples were  
28  
29 obtained by accumulation of 10, 100 and 1000 subsequent laser pulses per site with an incident  
30  
31 laser fluence of 40, 60, 80 and 100 mJ·cm<sup>-2</sup>. Two additional samples were prepared using 10000  
32  
33 pulses (100 mJ·cm<sup>-2</sup>) and 200 mJ·cm<sup>-2</sup> (1000 pulses).  
34  
35  
36  
37

38       **Synthesis of PbI<sub>2</sub> Single-walled Nanotubes by Thermal Treatment.** Steam purified and HCl  
39  
40 treated MWCNTs (6 mg) and PbI<sub>2</sub> (140 mg) were ground together with an agate mortar in a free  
41  
42 oxidant atmosphere and placed into a silica ampoule, evacuated and sealed under vacuum.  
43  
44 Afterward, the sample was annealed employing a 5 °C·min<sup>-1</sup> heating rate, dwelled at 500 °C for  
45  
46 12 h and cooled to room temperature. Additional samples were prepared by annealing  
47  
48 MWCNT/PbI<sub>2</sub> pellets, prepared as detailed above for the laser assisted synthesis, at 796 °C and  
49  
50 953 °C.  
51  
52  
53  
54  
55  
56  
57  
58  
59  
60

1  
2  
3 **Laser-assisted Synthesis of ZnI<sub>2</sub> Nanotubes.** 9 mg of purified MWCNTs were mixed with  
4 300 mg of ZnI<sub>2</sub> (Sigma-Aldrich) and well homogenized using an agate pestle and mortar inside  
5 an argon-filled glovebox. Pellets with 1.3 cm in diameter and ca. 0.5 mm in thickness were  
6 formed applying a pressure of 10 T to the MWCNT/ZnI<sub>2</sub> mixture. The pellet was irradiated as  
7 described above for PbI<sub>2</sub>.  
8  
9

10  
11  
12 **Sample Characterization.** Spots were characterized by Raman spectroscopy (Horiba Jobin  
13 Yvon) operating at 532 nm and using 100× objective. Acquisition time was set to 30 s and laser  
14 power to 0.5 mW. Spectra were obtained from several random places at each irradiated spot and  
15 fitted using OriginPro 8 software. Scanning electron microscopy characterization was performed  
16 on an FEI Magellan 400L at 5 kV, using a through-lens (TLD) detector for secondary electrons  
17 acquisition and a vCD detector optimized for high-contrast backscattered detection at low kV.  
18 Additionally the morphology of the irradiated spots was evaluated using high-angle annular dark  
19 field (HAADF) imaging in high resolution scanning transmission electron microscopy (STEM),  
20 carried out in a FEI Tecnai G2 F20 microscope operating at 200 kV. Samples were prepared by  
21 placing dropwise onto a lacey carbon support grid the dispersion obtained after sonication of a  
22 scratched fraction of the laser-irradiated area in hexane. Films morphology and resistance at the  
23 sub-micron scale was characterized by atomic force microscopy (AFM) using a 5500LS system  
24 from Agilent Technologies equipped with a Resiscope II module (CSI Instruments). Resistance  
25 maps were acquired in contact mode using diamond-coated silicon tips with a diameter of about  
26 100 nm. The resistance maps were acquired by applying 1 V between tip and sample. Current-  
27 voltage (I-V) spectroscopy analyses were also performed at specific locations of the samples by  
28 measuring the current flow through the tip in contact with the samples' surface while ranging the  
29  
30  
31  
32  
33  
34  
35  
36  
37  
38  
39  
40  
41  
42  
43  
44  
45  
46  
47  
48  
49  
50  
51  
52  
53  
54  
55  
56  
57  
58  
59  
60

1  
2  
3 applied voltage between -1 V and 1 V. The analysis of topographic and electric measurements  
4  
5 was carried out with the MountainsMap 7.0 software package from Digital Surf.  
6

7  
8 **Photothermal Simulation.** The temperature evolution of the MWCNT-PbI<sub>2</sub> composite  
9  
10 submitted to laser irradiation was modelled through a simple model composed by a carbon  
11  
12 nanotube immersed in a matrix of PbI<sub>2</sub>. The calculation was carried out by solving a 3D transient  
13  
14 heat conduction model by means of partial differential equations using COMSOL Multiphysics  
15  
16 5.3 software. Specific details on the photothermal simulation are included in the Supporting  
17  
18 Information.  
19  
20  
21  
22  
23  
24  
25  
26  
27  
28  
29  
30  
31  
32  
33  
34  
35  
36  
37  
38  
39  
40  
41  
42  
43  
44  
45  
46  
47  
48  
49  
50  
51  
52  
53  
54  
55  
56  
57  
58  
59  
60

## FIGURES

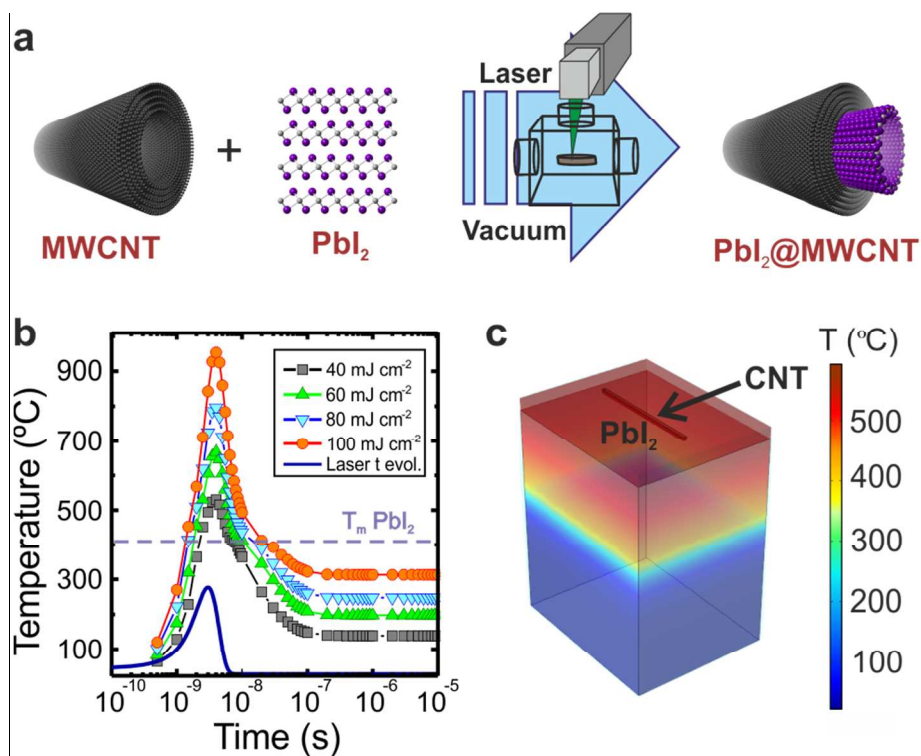


**Figure 1.** Laser-assisted filling of carbon nanotubes and photothermal simulation of the irradiated PbI<sub>2</sub>/MWCNT pellet. (a) Schematic representation of the laser-assisted filling of multi-walled carbon nanotubes. C, Pb and I atoms are represented by black, purple and grey spheres respectively. Note that bulk PbI<sub>2</sub> and the MWCNT are not schematically drawn in the same scale to better appreciate the layered crystal structure of bulk PbI<sub>2</sub>. The PbI<sub>2</sub>/MWCNT pellet (brown) is laser irradiated (plotted in green) inside the vacuum chamber. (b) Temporal evolution of the temperature of the pellet's surface upon irradiation with different laser fluences. The time evolution of the laser intensity is plotted for reference with a blue continuous line (a. u.). (c) 3D plot of temperature distribution in the MWCNT-PbI<sub>2</sub> system irradiated with 60 mJ·cm<sup>-2</sup> at 5 ns.

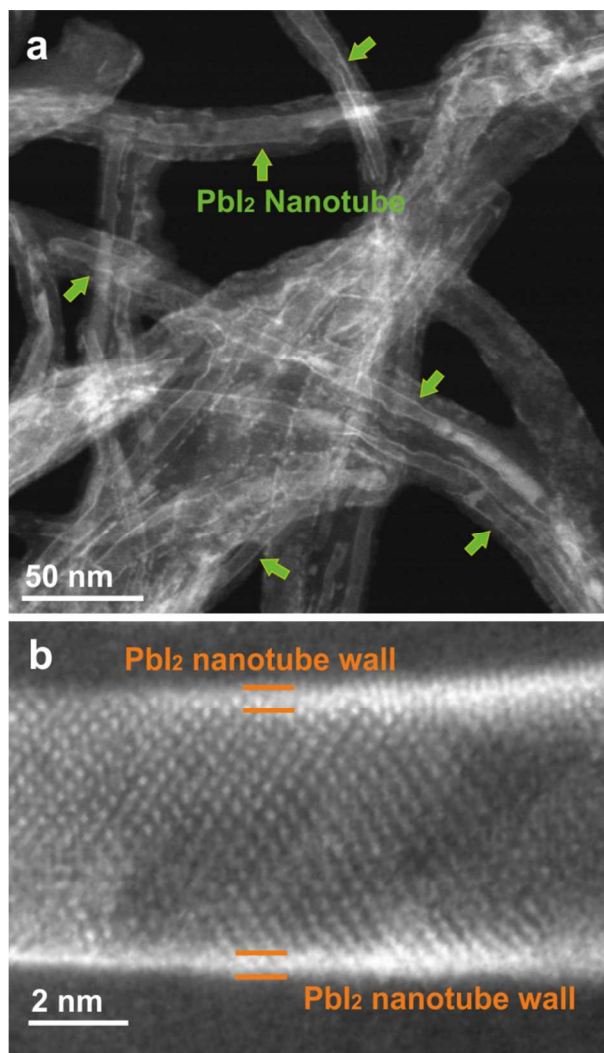


**Figure 2.** HAADF-STEM images of PbI<sub>2</sub>@MWCNTs prepared by laser irradiation employing an 80 mJ·cm<sup>-2</sup> fluence and 1000 pulses. (a) HAADF-STEM image (as prepared), (b) high resolution aberration corrected HAADF-STEM image (after one year of sample preparation). Green arrows in (a) point to well-defined single-walled inorganic PbI<sub>2</sub> nanotubes, while orange lines in (b) indicate the PbI<sub>2</sub> nanotube wall.

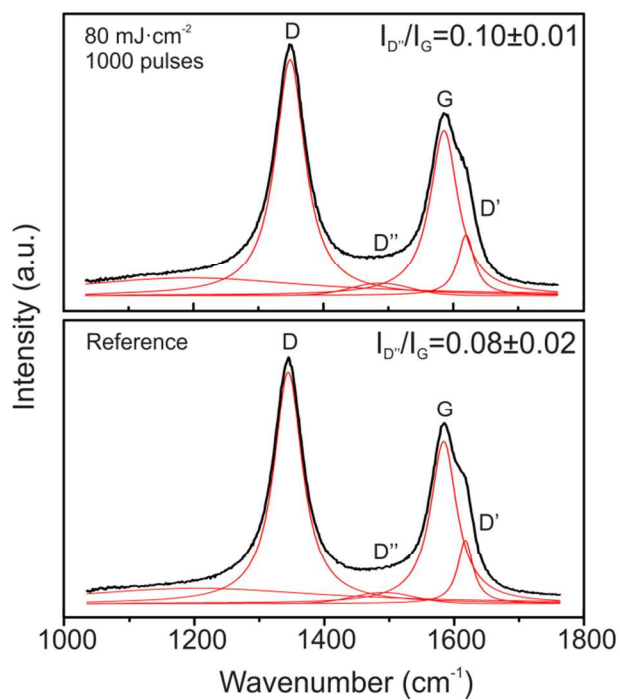


**Figure 3.** Deconvoluted Raman spectra acquired on PbI<sub>2</sub>/MWCNTs after laser irradiation employing 80 mJ·cm<sup>-2</sup> fluence and 1000 pulses and a non-irradiated area (reference). The experimental data curve and the fitting curves are shown in black and red respectively.



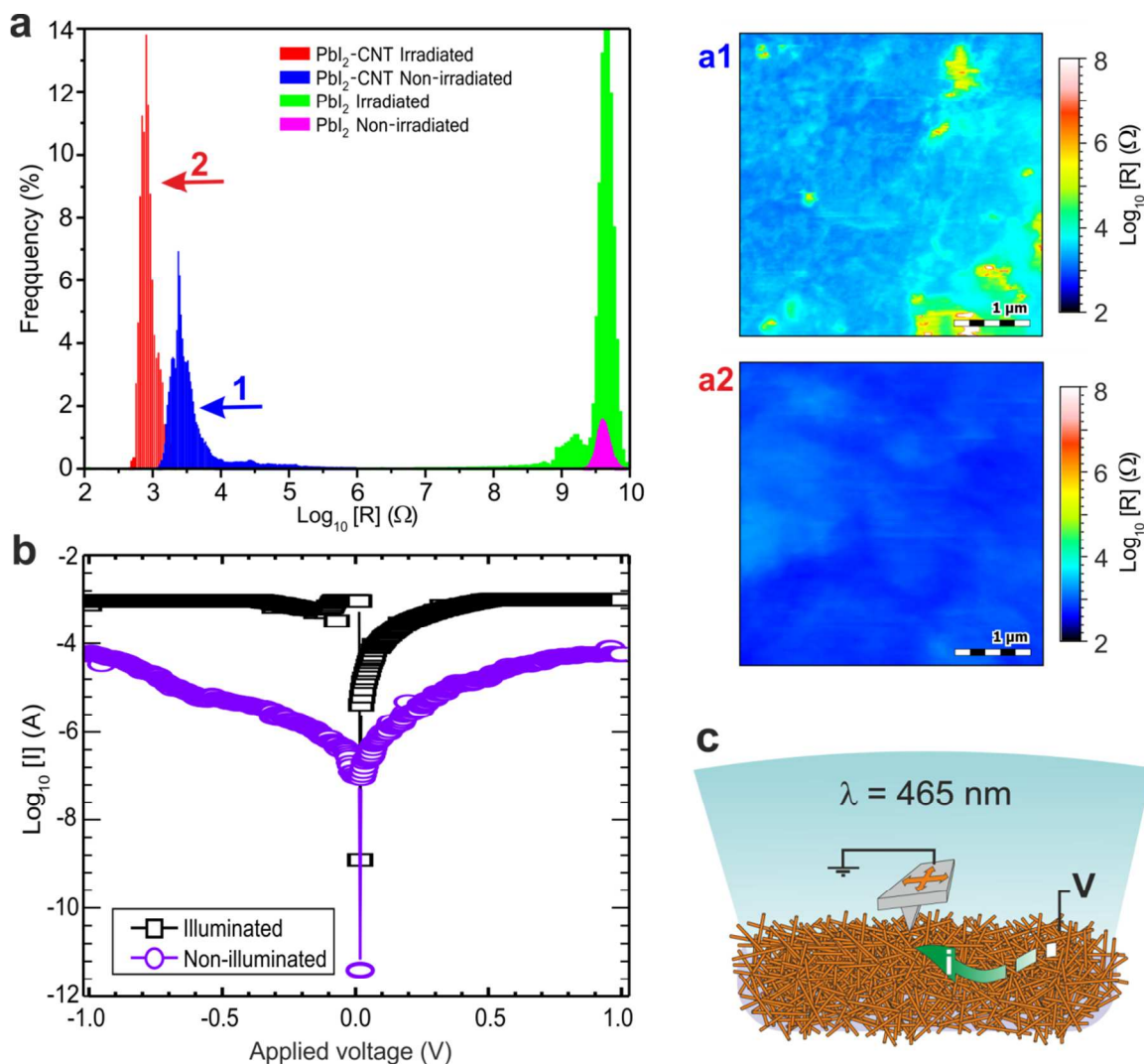


**Figure 4.** Conducting AFM measurements of  $\text{PbI}_2$  and  $\text{PbI}_2$ @MWCNTs pellets before and after laser irradiation with  $80 \text{ mJ} \cdot \text{cm}^{-2}$  and 1000 pulses. (a) Resistance map histograms. a1: resistance map of  $\text{PbI}_2$ @MWCNTs prior to irradiation; a2: resistance map of  $\text{PbI}_2$ @MWCNTs after irradiation. (b) Current-voltage spectroscopies of laser irradiated  $\text{PbI}_2$ @MWCNTs in dark conditions and illuminated with a blue LED (ca. 465 nm dominant wavelength). (c) Schematic representation of the experimental set-up employed for the conducting AFM measurements. Small orange cylinders represent  $\text{PbI}_2$ @MWCNTs.



**Figure 5.** HAADF-STEM image of ZnI<sub>2</sub>@MWCNT prepared by laser irradiation employing 100 mJ·cm<sup>-2</sup> fluence and 1000 pulses. The intensity profile along the red arrow is included on the right side of the image.

## ACKNOWLEDGMENTS

We acknowledge funding from MINECO (Spain), through MAT2017-86616-R, ENE2017-89210-C2-1-R and “Severo Ochoa” Programme for Centres of Excellence in R&D (SEV- 2015-0496, SEV-2013-0295), CERCA programme for funding ICN2 and support from AGAUR of Generalitat de Catalunya through the projects 2017 SGR 1086, 2017 SGR 581 and 2017 SGR 327. We thank Thomas Swan Co. Ltd. for supplying MWCNT Elicarb<sup>®</sup> samples. D. Kepić acknowledges financial support from the Ministry of Education, Science and Technological Development of the Republic of Serbia for postdoctoral research. We are grateful to R. Rurali (ICMAB-CSIC) for providing the structural model of the PbI<sub>2</sub> nanotube employed for the schematic representation of PbI<sub>2</sub>@MWCNT.

## ASSOCIATED CONTENT

The authors declare no competing financial interest.

### **Supporting Information.**

SEM, HAADF-STEM, stability studies and deconvoluted Raman spectra of laser irradiated PbI<sub>2</sub>/MWCNTs. HAADF-STEM of thermally annealed PbI<sub>2</sub>/MWCNTs. Statistical analysis of the number of MWCNTs walls. Details on the photothermal simulation. The Supporting Information is available free of charge on the ACS Publications website.

Supporting Information (PDF)

## AUTHOR INFORMATION

### **Corresponding Authors**

1  
2  
3 \*E-mail: gerard.tobias@icmab.es (G. Tobias), aperez@icmab.es (A. Perez),  
4 belen.ballesteros@icn2.cat (B.Ballesteros).  
5  
6  
7

### 8 **Author Contributions**

9

10  
11 S. Sandoval and D. Kepić contributed equally to this work.  
12  
13  
14  
15  
16  
17

### 18 **REFERENCES**

19

- 20  
21  
22 1. Duong, D. L.; Yun, S. J.; Lee, Y. H. Van der Waals Layered Materials: Opportunities and  
23 Challenges. *ACS Nano* **2017**, *11*, 11803-11830.  
24  
25  
26 2. Kelly, A. G.; Hallam, T.; Backes, C.; Harvey, A.; Esmaily, A. S.; Godwin, I.; Coelho, J.;  
27 Nicolosi, V.; Lauth, J.; Kulkarni, A.; Kinge, S.; Siebbeles, L. D. A.; Duesberg, G. S.; Coleman,  
28 J. N. All-Printed Thin-Film Transistors from Networks of Liquid-Exfoliated Nanosheets. *Science*  
29 **2017**, *356*, 69-73.  
30  
31  
32  
33 3. Hirunpinyopas, W.; Prestat, E.; Worrall, S. D.; Haigh, S. J.; Dryfe, R. A. W.; Bissett, M.  
34 A. Desalination and Nanofiltration through Functionalized Laminar MoS<sub>2</sub> Membranes. *ACS*  
35 *Nano* **2017**, *11*, 11082-11090.  
36  
37  
38 4. Zhang, C.; Anasori, B.; Seral-Ascaso, A.; Park, S.-H.; McEvoy, N.; Shmeliov, A.;  
39 Duesberg, G. S.; Coleman, J. N.; Gogotsi, Y.; Nicolosi, V. Transparent, Flexible, and  
40 Conductive 2D Titanium Carbide (Mxene) Films with High Volumetric Capacitance. *Adv.*  
41 *Mater.* **2017**, *29*, 1702678.  
42  
43  
44 5. Lai, Z.; Chen, Y.; Tan, C.; Zhang, X.; Zhang, H. Self-Assembly of Two-Dimensional  
45 Nanosheets into One-Dimensional Nanostructures. *Chem* **2016**, *1*, 59-77.  
46  
47  
48  
49  
50  
51  
52  
53  
54  
55  
56  
57  
58  
59  
60

- 1  
2  
3 6. Rafael, R.; Andrés, C.-G.; Emmanuele, C.; Francisco, G. Strain Engineering in  
4  
5 Semiconducting Two-Dimensional Crystals. *J. Phys. Condens. Mat.* **2015**, *27*, 313201.  
6
- 7  
8 7. Hwang, D. Y.; Choi, K. H.; Park, J. E.; Suh, D. H. Highly Thermal-Stable  
9  
10 Paramagnetism by Rolling up MoS<sub>2</sub> Nanosheets. *Nanoscale* **2017**, *9*, 503-508.  
11
- 12  
13 8. Mohammad, H. T.; Volker, J. S. Enhanced Photon Absorption in Spiral Nanostructured  
14  
15 Solar Cells Using Layered 2D Materials. *Nanotechnology* **2015**, *26*, 344005.  
16
- 17  
18 9. Liu, P.; Jin, Z.; Katsukis, G.; Drahushuk, L. W.; Shimizu, S.; Shih, C.-J.; Wetzal, E. D.;  
19  
20 Taggart-Scarff, J. K.; Qing, B.; Van Vliet, K. J.; Li, R.; Wardle, B. L.; Strano, M. S. Layered and  
21  
22 Scrolled Nanocomposites with Aligned Semi-Infinite Graphene Inclusions at the Platelet Limit.  
23  
24 *Science* **2016**, *353*, 364-367.  
25
- 26  
27 10. Gao, J.; Liu, X.; Zhang, G.; Zhang, Y.-W. Nanotube-Terminated Zigzag Edges of  
28  
29 Phosphorene Formed by Self-Rolling Reconstruction. *Nanoscale* **2016**, *8*, 17940-17946.  
30
- 31  
32 11. Soto Lamata, I.; Alonso-González, P.; Hillenbrand, R.; Nikitin, A. Y. Plasmons in  
33  
34 Cylindrical 2D Materials as a Platform for Nanophotonic Circuits. *ACS Photonics* **2015**, *2*, 280-  
35  
36 286.  
37
- 38  
39 12. Rao, C. N. R.; Govindaraj, A. Synthesis of Inorganic Nanotubes. *Adv. Mater.* **2009**, *21*,  
40  
41 4208-4233.  
42
- 43  
44 13. Višić, B.; Panchakarla, L. S.; Tenne, R. Inorganic Nanotubes and Fullerene-Like  
45  
46 Nanoparticles at the Crossroads between Solid-State Chemistry and Nanotechnology. *J. Am.*  
47  
48 *Chem. Soc.* **2017**, *139*, 12865-12878.  
49
- 50  
51 14. Jiang, J.; Meng, Y.; Zhang, L.; Liu, M. Self-Assembled Single-Walled Metal-Helical  
52  
53 Nanotube (M-H<sub>n</sub>): Creation of Efficient Supramolecular Catalysts for Asymmetric Reaction. *J.*  
54  
55 *Am. Chem. Soc.* **2016**, *138*, 15629-15635.  
56  
57  
58  
59  
60

- 1  
2  
3 15. Liu, H.; Li, H.; Wang, X. Electrostatic Interaction-Directed Growth of Nickel Phosphate  
4 Single-Walled Nanotubes for High Performance Oxygen Evolution Reaction Catalysts. *Small*  
5 **2016**, *12*, 2969-2974.  
6  
7
- 8  
9  
10 16. Ni, B.; Liu, H.; Wang, P.-P.; He, J.; Wang, X. General Synthesis of Inorganic Single-  
11 Walled Nanotubes. *Nat. Commun.* **2015**, *6*, 8756.  
12  
13
- 14  
15 17. Cabana, L.; Ballesteros, B.; Batista, E.; Magén, C.; Arenal, R.; Oró-Solé, J.; Rurali, R.;  
16 Tobias, G. Synthesis of PbI<sub>2</sub> Single-Layered Inorganic Nanotubes Encapsulated within Carbon  
17 Nanotubes. *Adv. Mater.* **2014**, *26*, 2016–2021.  
18  
19
- 20  
21 18. Sandoval, S.; Pach, E.; Ballesteros, B.; Tobias, G. Encapsulation of Two-Dimensional  
22 Materials inside Carbon Nanotubes: Towards an Enhanced Synthesis of Single-Layered Metal  
23 Halides. *Carbon* **2017**, *123*, 129-134.  
24  
25
- 26  
27 19. Toth, P. S.; Velický, M.; Bissett, M. A.; Slater, T. J. A.; Savjani, N.; Rabiou, A. K.;  
28 Rakowski, A. M.; Brent, J. R.; Haigh, S. J.; O'Brien, P.; Dryfe, R. A. W. Asymmetric  
29 MoS<sub>2</sub>/Graphene/Metal Sandwiches: Preparation, Characterization, and Application. *Adv. Mater.*  
30 **2016**, *28*, 8256-8264.  
31  
32
- 33  
34 20. Novoselov, K. S.; Mishchenko, A.; Carvalho, A.; Castro Neto, A. H. 2D Materials and  
35 van der Waals Heterostructures. *Science* **2016**, *353*, aac9439.  
36  
37
- 38  
39 21. Roy, K.; Ahmed, T.; Dubey, H.; Sai, T. P.; Kashid, R.; Maliakal, S.; Hsieh, K.; Shamim,  
40 S.; Ghosh, A. Number-Resolved Single-Photon Detection with Ultralow Noise van der Waals  
41 Hybrid. *Adv. Mater.* **2018**, *30*, 1704412.  
42  
43
- 44  
45 22. Roy, K.; Padmanabhan, M.; Goswami, S.; Sai, T. P.; Ramalingam, G.; Raghavan, S.;  
46 Ghosh, A. Graphene-MoS<sub>2</sub> Hybrid Structures for Multifunctional Photoresponsive Memory  
47 Devices. *Nat. Nanotechnol.* **2013**, *8*, 826-830.  
48  
49  
50  
51  
52  
53  
54  
55  
56  
57  
58  
59  
60

- 1  
2  
3 23. Chaudhary, S. K. Lead Iodide Crystals as Input Material for Radiation Detectors. *Cryst.*  
4  
5 *Struct. Theor. App.* **2012**, *1*, 21-24.  
6  
7  
8 24. Li, W.; Wang, Z.; Deschler, F.; Gao, S.; Friend, R. H.; Cheetham, A. K. Chemically  
9  
10 Diverse and Multifunctional Hybrid Organic–Inorganic Perovskites. *Nat. Mater. Rev.* **2017**, *2*,  
11  
12 16099.  
13  
14 25. Zhou, M.; Duan, W.; Chen, Y.; Du, A. Single Layer Lead Iodide: Computational  
15  
16 Exploration of Structural, Electronic and Optical Properties, Strain Induced Band Modulation  
17  
18 and the Role of Spin-Orbital-Coupling. *Nanoscale* **2015**, *7*, 15168-15174.  
19  
20  
21 26. Zhong, M.; Zhang, S.; Huang, L.; You, J.; Wei, Z.; Liu, X.; Li, J. Large-Scale 2D PbI<sub>2</sub>  
22  
23 Monolayers: Experimental Realization and Their Indirect Band-Gap Related Properties.  
24  
25 *Nanoscale* **2017**, *9*, 3736-3741.  
26  
27  
28 27. Botos, A.; Biskupek, J.; Chamberlain, T. W.; Rance, G. A.; Stoppiello, C. T.; Sloan, J.;  
29  
30 Liu, Z.; Suenaga, K.; Kaiser, U.; Khlobystov, A. N. Carbon Nanotubes as Electrically Active  
31  
32 Nanoreactors for Multi-Step Inorganic Synthesis: Sequential Transformations of Molecules to  
33  
34 Nanoclusters and Nanoclusters to Nanoribbons. *J. Am. Chem. Soc.* **2016**, *138*, 8175-8183.  
35  
36  
37 28. Spencer, J. H.; Nesbitt, J. M.; Trehwitt, H.; Kashtiban, R. J.; Bell, G.; Ivanov, V. G.;  
38  
39 Faulques, E.; Sloan, J.; Smith, D. C. Raman Spectroscopy of Optical Transitions and Vibrational  
40  
41 Energies of ~1 nm HgTe Extreme Nanowires within Single Walled Carbon Nanotubes. *ACS*  
42  
43 *Nano* **2014**, *8*, 9044-9052.  
44  
45  
46 29. Chamberlain, T. W.; Biskupek, J.; Skowron, S. T.; Markevich, A. V.; Kurasch, S.;  
47  
48 Reimer, O.; Walker, K. E.; Rance, G. A.; Feng, X.; Müllen, K.; Turchanin, A.; Lebedeva, M. A.;  
49  
50 Majouga, A. G.; Nenajdenko, V. G.; Kaiser, U.; Besley, E.; Khlobystov, A. N. Stop-Frame  
51  
52  
53  
54  
55  
56  
57  
58  
59  
60

1  
2  
3 Filming and Discovery of Reactions at the Single-Molecule Level by Transmission Electron  
4  
5 Microscopy. *ACS Nano* **2017**, *11*, 2509-2520.

6  
7  
8 30. Meyer, R. R.; Sloan, J.; Dunin-Borkowski, R. E.; Kirkland, A. I.; Novotny, M. C.;  
9  
10 Bailey, S. R.; Hutchison, J. L.; Green, M. L. H. Discrete Atom Imaging of One-Dimensional  
11  
12 Crystals Formed within Single-Walled Carbon Nanotubes. *Science* **2000**, *289*, 1324-1326.

13  
14  
15 31. Cambré, S.; Santos, S. M.; Wenseleers, W.; Nugraha, A. R. T.; Saito, R.; Cognet, L.;  
16  
17 Lounis, B. Luminescence Properties of Individual Empty and Water-Filled Single-Walled  
18  
19 Carbon Nanotubes. *ACS Nano* **2012**, *6*, 2649-2655.

20  
21  
22 32. Chaban, V. V.; Prezhdo, V. V.; Prezhdo, O. V. Confinement by Carbon Nanotubes  
23  
24 Drastically Alters the Boiling and Critical Behavior of Water Droplets. *ACS Nano* **2012**, *6*, 2766-  
25  
26 2773.

27  
28  
29 33. Agrawal, K. V.; Shimizu, S.; Drahushuk, L. W.; Kilcoyne, D.; Strano, M. S. Observation  
30  
31 of Extreme Phase Transition Temperatures of Water Confined inside Isolated Carbon Nanotubes.  
32  
33 *Nat. Nanotechnol.* **2016**, *12*, 267.

34  
35  
36 34. Sloan, J.; Matthewman, G.; Dyer-Smith, C.; Sung, A. Y.; Liu, Z.; Suenaga, K.; Kirkland,  
37  
38 A. I.; Flahaut, E. Direct Imaging of the Structure, Relaxation, and Sterically Constrained Motion  
39  
40 of Encapsulated Tungsten Polyoxometalate Lindqvist Ions within Carbon Nanotubes. *ACS Nano*  
41  
42 **2008**, *2*, 966-976.

43  
44  
45 35. Khlobystov, A. N. Carbon Nanotubes: From Nano Test Tube to Nano-Reactor. *ACS*  
46  
47 *Nano* **2011**, *5*, 9306-9312.

48  
49  
50 36. Liu, X.; Marangon, I.; Melinte, G.; Wilhelm, C.; Ménard-Moyon, C.; Pichon, B. P.;  
51  
52 Ersen, O.; Aubertin, K.; Baaziz, W.; Pham-Huu, C.; Bégin-Colin, S.; Bianco, A.; Gazeau, F.;  
53  
54 Bégin, D. Design of Covalently Functionalized Carbon Nanotubes Filled with Metal Oxide  
55  
56  
57  
58  
59  
60



1  
2  
3 Nanoparticles for Imaging, Therapy, and Magnetic Manipulation. *ACS Nano* **2014**, *8*, 11290-  
4 11304.

5  
6  
7  
8 37. Stoppiello, C. T.; Biskupek, J.; Li, Z. Y.; Rance, G. A.; Botos, A.; Fogarty, R. M.;  
9 Bourne, R. A.; Yuan, J.; Lovelock, K. R. J.; Thompson, P.; Fay, M. W.; Kaiser, U.;  
10 Chamberlain, T. W.; Khlobystov, A. N. A One-Pot-One-Reactant Synthesis of Platinum  
11 Compounds at the Nanoscale. *Nanoscale* **2017**, *9*, 14385-14394.

12  
13  
14  
15 38. Wang, Z.; Li, H.; Liu, Z.; Shi, Z.; Lu, J.; Suenaga, K.; Joung, S. K.; Okazaki, T.; Gu, Z.;  
16 Zhou, J.; Gao, Z.; Li, G.; Sanvito, S.; Wang, E.; Iijima, S. Mixed Low-Dimensional  
17 Nanomaterial: 2D Ultranarrow MoS<sub>2</sub> Inorganic Nanoribbons Encapsulated in Quasi-1D Carbon  
18 Nanotubes. *J. Am. Chem. Soc.* **2010**, *132*, 13840-13847.

19  
20  
21  
22 39. Sloan, J.; Kirkland, A. I.; Hutchison, J. L.; Green, M. L. H. Integral Atomic Layer  
23 Architectures of 1D Crystals Inserted into Single Walled Carbon Nanotubes. *Chem. Commun.*  
24 **2002**, 1319-1332.

25  
26  
27  
28 40. Eliseev, A. A.; Verbitskiy, N. I.; Volykhov, A. A.; Fedorov, A. V.; Vilkov, O. Y.;  
29 Verbitskiy, I. I.; Brzhezinskaya, M. M.; Kiselev, N. A.; Yashina, L. V. The Impact of  
30 Dimensionality and Stoichiometry of CuBr on Its Coupling to sp<sup>2</sup>-Carbon. *Carbon* **2016**, *99*,  
31 619-623.

32  
33  
34  
35 41. Ilie, A.; Bendall, J. S.; Nagaoka, K.; Egger, S.; Nakayama, T.; Crampin, S. Encapsulated  
36 Inorganic Nanostructures: A Route to Sizable Modulated, Noncovalent, on-Tube Potentials in  
37 Carbon Nanotubes. *ACS Nano* **2011**, *5*, 2559-2569.

38  
39  
40  
41 42. Handbook of Chemistry and Physics. 84<sup>th</sup> ed.; CRC Press: 2003-2004.

42  
43  
44  
45 43. Nellist, P. D.; Pennycook, S. J. Direct Imaging of the Atomic Configuration of  
46 Ultradispersed Catalysts. *Science* **1996**, *274*, 413-415.

- 1  
2  
3 44. Palosz, B. The Structure of  $\text{PbI}_2$  Polytypes 2H and 4H: A Study of the 2H-4H Transition.  
4  
5 *J. Phys.: Condens. Matter* **1990**, *2*, 5285.  
6  
7  
8 45. Kreizman, R.; Enyashin, A. N.; Deepak, F. L.; Albu-Yaron, A.; Popovitz-Biro, R.;  
9  
10 Seifert, G.; Tenne, R. Synthesis of Core–Shell Inorganic Nanotubes. *Adv. Funct. Mater.* **2010**,  
11  
12 *20*, 2459-2468.  
13  
14  
15 46. Kreizman, R.; Hong, S. Y.; Sloan, J.; Popovitz-Biro, R.; Albu-Yaron, A.; Tobias, G.;  
16  
17 Ballesteros, B.; Davis, B. G.; Green, M. L. H.; Tenne, R. Core–Shell  $\text{PbI}_2@WS_2$  Inorganic  
18  
19 Nanotubes from Capillary Wetting. *Angew. Chem. Int. Ed.* **2009**, *48*, 1230-1233.  
20  
21  
22 47. Pérez del Pino, Á.; György, E.; Cabana, L.; Ballesteros, B.; Tobias, G. Ultraviolet Pulsed  
23  
24 Laser Irradiation of Multi-Walled Carbon Nanotubes in Nitrogen Atmosphere. *J. Appl. Phys.*  
25  
26 **2014**, *115*, 093501.  
27  
28  
29 48. Flahaut, E.; Sloan, J.; Friedrichs, S.; Kirkland, A. I.; Coleman, K. S.; Williams, V. C.;  
30  
31 Hanson, N.; Hutchison, J. L.; Green, M. L. H. Crystallization of 2H and 4H  $\text{PbI}_2$  in Carbon  
32  
33 Nanotubes of Varying Diameters and Morphologies. *Chem. Mater.* **2006**, *18*, 2059-2069.  
34  
35  
36 49. Enyashin, A. N.; Kreizman, R.; Seifert, G. Capillary Imbibition of  $\text{PbI}_2$  Melt by Inorganic  
37  
38 and Carbon Nanotubes. *J. Phys. Chem. C* **2009**, *113*, 13664-13669.  
39  
40  
41 50. Nair, R. R.; Blake, P.; Grigorenko, A. N.; Novoselov, K. S.; Booth, T. J.; Stauber, T.;  
42  
43 Peres, N. M. R.; Geim, A. K. Fine Structure Constant Defines Visual Transparency of Graphene.  
44  
45 *Science* **2008**, *320*, 1308-1308.  
46  
47  
48 51. Dou, L.; Cui, F.; Yu, Y.; Khanarian, G.; Eaton, S. W.; Yang, Q.; Resasco, J.;  
49  
50 Schildknecht, C.; Schierle-Arndt, K.; Yang, P. Solution-Processed Copper/Reduced-Graphene-  
51  
52 Oxide Core/Shell Nanowire Transparent Conductors. *ACS Nano* **2016**, *10*, 2600-2606.  
53  
54  
55  
56  
57  
58  
59  
60

- 1  
2  
3 52. Cabana, L.; Ke, X.; Kepić, D.; Oro-Solé, J.; Tobías-Rossell, E.; Van Tendeloo, G.;  
4 Tobias, G. The Role of Steam Treatment on the Structure, Purity and Length Distribution of  
5 Multi-Walled Carbon Nanotubes. *Carbon* **2015**, *93*, 1059-1067.  
6  
7  
8  
9

10  
11 TABLE OF CONTENTS  
12

